RSC Advances

PAPER

View Article Online
View Journal | View Issue

Cite this: *RSC Adv.*, 2025, **15**, 3089

Construction of a hydrazine electrochemical sensor using Ag@ZIF as the electrode material†

Praveen Kumar,‡*[a] Saood Ali,‡*[b] Khursheed Ahmad,*[c] Waseem Raza[d] and Rais Ahmad Khan[e]

Received 4th November 2024
Accepted 13th December 2024

DOI: 10.1039/d4ra07849g

rsc.li/rsc-advances

In recent years, the fabrication of hydrazine sensors has received extensive attention because of the toxicity of hydrazine to the environment and human beings. It is thus important to design and develop efficient electrode modifiers for the construction of hydrazine electrochemical sensors. Herein, we reported the benign synthesis of a silver (Ag)-doped zinc-based zeolitic imidazolate framework (ZIF-8). The synthesized Ag@ZIF-8 was characterized by various advanced physiochemical characterization methods, including X-ray diffraction (XRD), scanning electron microscopy (SEM), and energy dispersive X-ray spectroscopy (EDX). A screen-printed electrode (SPE) was modified with the prepared Ag@ZIF-8. The cyclic voltammetry (CV) and linear sweep voltammetry (LSV) methods were used for assessing its sensing towards hydrazine. The obtained results showed a reasonable detection limit (0.1 μM), sensitivity (1.98 μA μM cm^{-2}), stability, selectivity, and repeatability using Ag@ZIF-8/SPE as a hydrazine sensor. The real-sample investigations demonstrated recovery rates of 96–97%.

1. Introduction

Hydrazine is a strong reducing agent and has been widely used in various applications, such as rocket fuel propellants, fuel cells, and herbicides.[1–3] The by-products of hydrazine are also used as intermediates or chemical blowing agents in pharmaceutical industries.[4–6] Even though hydrazine offers several advantageous properties for its use in various applications and industries, its carcinogenic nature is one of the major concerns.[7–9] Hydrazine has negative impacts on human beings owing to its instability and hypertoxicity.[8] Hydrazine may cause serious damage to human health, such as nausea, dizziness, bronchitis, seizures, temporary blindness, headache, eye irritation, dermatitis, liver, kidney disease, and central nervous system issues.[9–11] Thus, there is a need for the precise and selective determination of hydrazine.[12,13] In this context, various conventional methods, such as titrimetry, coulometry, amperometry, potentiometry, spectrophotometry, and chromatography, have been developed for the monitoring of hydrazine.[14–18] Although, these conventional approaches can be used as sensing platforms for monitoring the accurate level of hydrazine, they typically suffer from various disadvantages, such as being time consuming, needing a sophisticated room for the instruments, high cost of the instruments, and the need for well-trained operators.[19] Thus, a low cost, sensitive, selective, and environmentally friendly method is required for the monitoring of hydrazine. In this regard, electrochemical methods have been developed for the determination of hydrazine and various toxic molecules. Electrochemical methods have received extensive attention because of their excellent sensitivity, selectivity, portability, eco-friendliness, cost-effectiveness, and fast response.[19–22]

In previous years, electrochemical sensing techniques have been considered as one of the efficient approaches for the determination of various molecules.[18–23] Electrode materials play a crucial role in electrochemical sensing technology.[20] Chemically modified electrodes are used as the working electrode, in which nanomaterials, polymers, and metal–organic frameworks (MOFs) are widely used as the electrode materials.[24–26] MOFs possess a high surface area and porosity, which are beneficial for better electron–transport reactions.[27–29] In particular, zeolite imidazolate framework (ZIF) materials are a subgroup of MOFs in which four coordinated transition metals are interconnected with imidazolate units.[30–32] ZIF materials have been used in gas adsorption, molecular separation, catalysis, and chemical sensing.[33–35] ZIF-8 is a zinc-based material in which Zn^{2+} cations are connected *via* bridging 2-

[a]*Department of Chemistry, Indian Institute of Technology Indore, Simrol, Khandwa Road, MP, 453552, India*

[b]*School of Mechanical Engineering, Yeungnam University, Gyeongsan 38541, Republic of Korea*

[c]*School of Materials Science and Engineering, Yeungnam University, Gyeongsan 38541, Republic of Korea. E-mail: khursheed.energy@gmail.com*

[d]*Department of Materials Science and Engineering, WW4-LKO, University of ErlangenNuremberg, Martensstrasse 7, 91058 Erlangen, Germany*

[e]*Department of Chemistry, College of Science, King Saud University, Riyadh, 11451, Kingdom of Saudi Arabia*

† Electronic supplementary information (ESI) available. See DOI: https://doi.org/10.1039/d4ra07849g

‡ Equal contribution.

methylimidazole anions and form a three-dimensional (3D) structure.[34] The reported literature suggests that the sensing performance of ZIF-8 can be further improved by doping with transition metal ions.[35] In this regard, Huang *et al.*[35] reported the fabrication of nitrogen-doped ZIF-8 for the sensing of cadmium. In another report, Fatima *et al.*[36] synthesized tellurium-doped ZIF-8 for the sensing of hydrogen peroxide. Thus, it can be understood that doping may enhance the catalytic properties of ZIF-8 for electrochemical sensing applications. Silver (Ag) has excellent catalytic and conductive properties, and stability.[37,38] Ag-anchored ZIF-8 may show better synergistic interactions and catalytic behavior for the determination of hydrazine.

In the present study, we synthesized Ag@ZIF-8 by employing simple strategies optimized in our research group. Subsequently, a screen-printed carbon electrode (SPE) was modified using Ag@ZIF-8 as a catalyst. This modified electrode, referred to as Ag@ZIF-8/SPE, was then utilized as a sensor for detecting hydrazine. Our detection methodology involved employing cyclic voltammetry (CV) and linear sweep voltammetry (LSV) for the accurate and reliable quantification of hydrazine.

2. Materials and methods

2.1. Materials

Zinc nitrate hexahydrate ($Zn(NO_3)_2 \cdot 6H_2O$; reagent grade, 98%), silver nitrate (ACS reagent, ≥99.0%), and 2-methylimidazole (2-MIM; 99%) were bought from Merck. Methanol and ethanol were purchased from Sigma. Hydrazine, glucose, hydrogen peroxide (H_2O_2; 30% (w/w) in H_2O), ascorbic acid (99%), *para*-nitrophenol (≥99%), uric acid (≥99%), urea (ACS reagent, 99.0%), citric acid (≥99.5%), and ammonia were bought from Sigma-Aldrich and Merck. All the materials were of analytical grade and used without any further purification.

2.2. Instrumental

The X-ray powder diffraction patterns of the prepared samples were collected on a Bruker D8 advance diffractometer (Cu Kα radiation) within the 2theta range of 5–80°. The morphological features, such as SEM images of the prepared samples, were collected on a Hitachi, S-4800 scanning electrode microscope. The elemental composition study (energy dispersive X-ray spectroscopic; EDX) was performed on a Horiba instrument. The X-ray photoelectron spectroscopy (XPS) data were obtained on a Thermo Fischer-Scientific instrument. The sensing experiments, such as cyclic voltammetry (CV) and LSV, were performed using an electrode system (CH instrument). The three-electrode system comprised a working electrode (SPE), reference electrode (Ag/AgCl), and counter electrode (Pt wire). Phosphate buffer saline solution (PBS) of pH 7.0 was used for all the electrochemical measurements.

2.3. Synthesis of Ag@ZIF-8

ZIF-8 and Ag@ZIF-8 were synthesized at room temperature (RT). In brief, 1.2 g zinc nitrate hexahydrate was dissolved in 75 mL methanol. Next, 2.6 g of 2-methylimidazole (2-MIM) was dissolved in another beaker containing 75 mL methanol. Both the prepared solutions were carefully and slowly mixed with continuous stirring at RT for 120 min. A white-colored precipitate was obtained by filtration of the reaction solution and dried at 60–70 °C overnight. The prepared sample was labeled as ZIF-8.

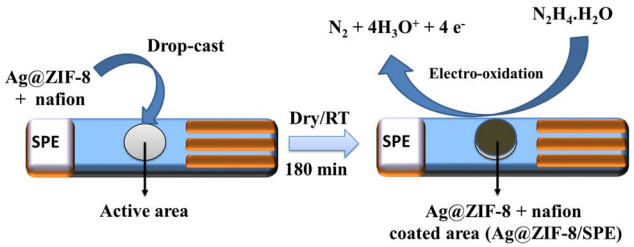

Scheme 1 Schematic for the fabrication of Ag@ZIF-8/SPE for hydrazine sensing.

For the synthesis of Ag@ZIF-8, 0.1 g of silver nitrate was added to 25 mL methanol and stirred at RT to completely dissolve the silver nitrate. Further, 0.5 g of the as-prepared ZIF-8 was dispersed into the silver nitrate solution and stirred for 60 min under a halogen lamp. The prepared sample (Ag@ZIF-8) was separated using the centrifugation method and washed with ethanol to remove the adsorbed residual impurities. The Ag@ZIF-8 was dried at 60 °C overnight in a vacuum oven.

2.4. Fabrication of the SPE

The SPE surface was coated with the as-prepared ZIF-8 or Ag@ZIF-8 catalyst by a drop-casting method. Typically, 1.5 mg of the catalyst (ZIF-8 or Ag@ZIF-8) was dispersed in 2 mL deionized (DI) water (0.5 wt% Nafion as binder) using ultrasonication for 30 min. The prepared ink (7 μL) was drop-cast on the surface of the SPE and dried at RT for 180 min (Scheme 1). The ZIF-8- and Ag@ZIF-8-modified electrodes were labeled as ZIF-8/SPE and Ag@ZIF-8/SPE, respectively.

3. Results and discussion

3.1. Materials characterizations

Powder X-ray diffraction (PXRD) is one of the most significant physiochemical techniques to study the phase purity, crystallinity, and structure of materials. The PXRD pattern of the prepared ZIF-8 and Ag@ZIF-8 were recorded in the two-theta range of 5–80°. Fig. 1a presents the obtained PXRD patterns of the ZIF-8 and Ag@ZIF-8 samples. ZIF-8 exhibited the presence of various diffraction peaks, which were well-matched with the calculated PXRD pattern of the ZIF-8, as shown in Fig. 1a. The major diffraction peaks at 2theta values of 7.32°, 10.40°, 12.69°, 14.68°, 16.40°, 18.14°, 24.44°, 26.61°, and 29.58° could be indexed to the presence of (011), (002), (112), (022), (013), (222), (114), (134), and (044) diffraction planes, respectively. This obtained data confirmed the formation of ZIF-8, while strong diffraction peaks revealed the decent crystalline nature of the prepared ZIF-8. The XRD pattern of the ZIF-8 was in agreement with the previous reported literature.[39]

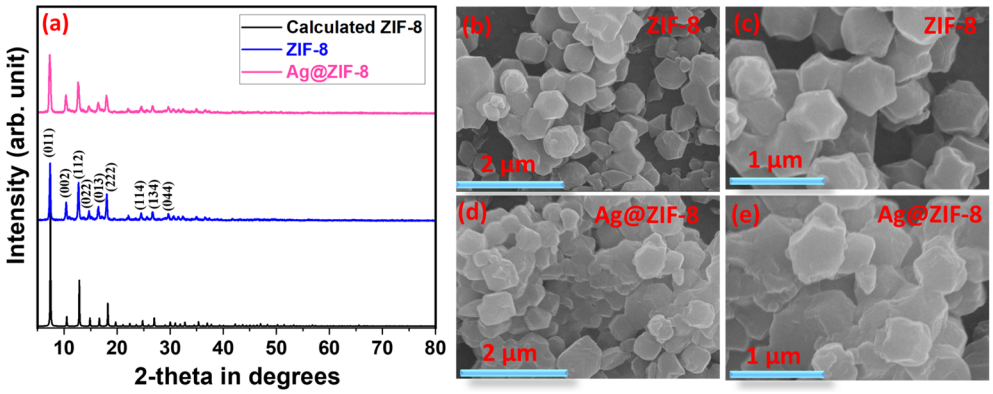

Fig. 1 (a) XRD patterns of ZIF-8 and Ag@ZIF-8. FE-SEM images of ZIF-8 (b and c) and Ag@ZIF-8 (d and e) at different magnifications.

In the prepared Ag@ZIF-8 sample, diffraction planes of (011), (002), (112), (022), (013), (222), (114), (134), and (044) were observed, which were attributed to the presence of ZIF material in the synthesized Ag@ZIF-8. However, no peak for Ag was observed. This may be due to the presence of only a low concentration of the Ag in the prepared Ag@ZIF-8 sample. Ag@ZIF-8 also possessed a crystalline nature with strong diffraction peaks and high intensity. The obtained XRD results were in good agreement with previously reported literature.[39] The surface structure of materials plays a crucial role in electron transportation, and catalysis. Thus, evaluation of the surface structural properties of the as-synthesized ZIF-8 and Ag@ZIF-8 is of great significance. In this regard, the surface morphological characteristics of the prepared ZIF-8 and Ag@ZIF-8 were checked using a SEM method. Fig. 1b and c display the FE-SEM images of the prepared ZIF-8, which revealed that ZIF-8 comprised a uniform rhombic dodecahedral structure with particle sizes of less than 1 μm with a distinct crystal surface. Fig. 1d and e present the FE-SEM pictures of Ag@ZIF-8. It could be observed from the obtained SEM images that Ag-doping affected the morphological features of the Ag@ZIF-8 sample. Agglomeration could be seen in the prepared Ag@ZIF-8 sample, which may be due to the Ag-doping.

The PXRD and SEM data of ZIF-8 and Ag@ZIF-8 revealed their good phase purity, crystallinity and surface structural characteristics, but the presence of Ag in the prepared Ag@ZIF-8 could not be confirmed. Therefore, this required further analysis to authenticate the successful Ag-doping in the prepared Ag@ZIF-8 sample. Therefore, EDX was performed and the spectra of ZIF-8 and Ag@ZIF-8 were recorded and are shown in Fig. 2a. Fig. 2a exhibits the presence of EDX signals for C, N, Zn, and O elements in the ZIF-8 sample. This showed that ZIF-8 has decent phase purity. Similarly, the EDX spectrum of the prepared Ag@ZIF-8 showed the presence of C, N, Zn, Ag, and O elements. This confirmed that Ag was present in the prepared Ag@ZIF-8 sample, as shown in Fig. 2. Additionally, elemental mapping was utilized to visualize the distribution of Ag in ZIF-8, as depicted in Fig. 2b–g. The EDX mapping results for the prepared Ag@ZIF-8 sample are shown in Fig. 2b–g. The EDX mapping results indicated the uniform particle distribution of Zn, Ag, N, O, and C elements, as shown in Fig. 2c–g, respectively. The EDX results suggested the incorporation of Ag in the prepared Ag@ZIF-8 sample. The outcomes of elemental mapping provide further confirmation, distinctly indicating the presence of Ag in Ag@ZIF-8 sample. This visualization strengthens the evidence of successful Ag loading in Ag@ZIF-8, corroborating the findings from the elemental analysis.

In further investigations, we also used XPS to further confirm the presence of Ag in the prepared Ag@ZIF-8 sample. The recorded XPS survey scan of the prepared Ag@ZIF-8 sample is displayed in Fig. S1a.† The survey spectrum revealed the presence of C, N, Ag, Zn, and O elements. Thus, it can be clearly understood that Ag was introduced in to the ZIF-8. The high-resolution XPS scan of Zn 2p is shown in Fig. S1b,† while that for Ag 3d is presented in Fig. S1c.† The Zn 2p demonstrated the presence of two XPS peaks, which corresponded to the presence of Zn $2p_{1/2}$ and Zn $2p_{3/2}$, respectively (Fig. S1b†). Two XPS peaks were also observed in the Ag 3d spectrum, which could be assigned to the presence of Ag $3d_{3/2}$ and Ag $3d_{5/2}$, respectively (Fig. S1c†). The above results confirmed the formation of Ag@ZIF-8.

3.2. Hydrazine sensor

Hydrazine can be effectively detected by using electrochemical sensing technology, which may involve the electro-oxidation of hydrazine. We adopted a three-electrode setup to determine hydrazine using cyclic voltammetry (CV). The CV curves of the SPE, ZIF-8/SPE, and Ag@ZIF-8/SPE were thus obtained for 0.5 μM hydrazine (prepared in 0.1 M PBS of pH 7.0) at an applied scan rate of 25 mV s^{-1}. The observations showed the electro-oxidation of hydrazine at the surface of the SPE with a current response of 1.7 μA, as shown in Fig. 3a. The CV data of the ZIF-8/SPE showed some improvements in the electro-oxidation of hydrazine. Thus, an enhanced current value of 2.34 μA was observed for the electro-oxidation of hydrazine at the surface of ZIF-8/SPE. Furthermore, significant changes in the current response of Ag@ZIF-8/SPE were observed and an interesting current response of 3.41 μA was obtained for the electrochemical oxidation of hydrazine. This may be attributed to the excellent electrocatalytic properties of the Ag@ZIF-8 catalyst.

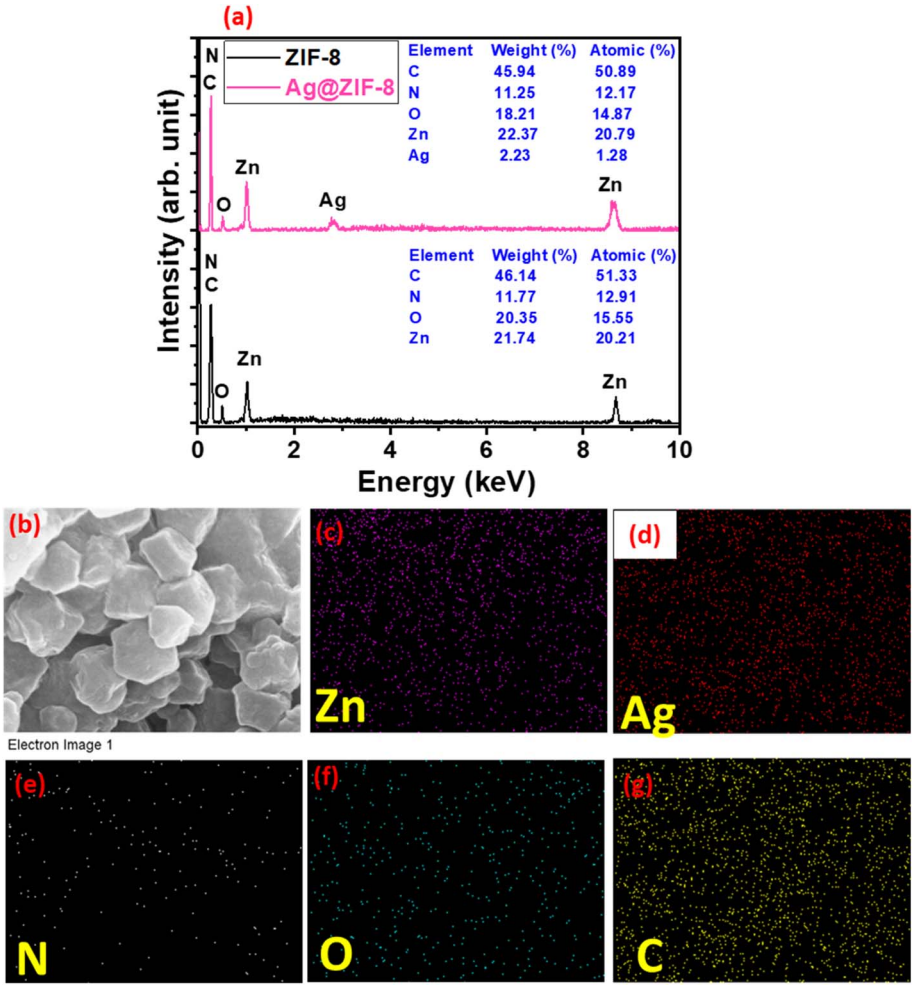

Fig. 2 (a) EDX spectra of ZIF-8 and Ag@ZIF-8. EDX electron image (b), and mapping images for Zn (c), Ag (d), N (e), O (f), and C (g) in the prepared Ag@ZIF-8.

The above discussion mentions that Ag@ZIF-8/SPE had higher electrocatalytic properties compared to the SPE or ZIF-8/SPE. This indicates that the introduction of Ag further enhanced the catalytic properties of Ag@ZIF-8. The CV responses of the SPE and Ag@ZIF-8/SPE were also studied in the presence of 0.1 M PBS of pH 7.0 at a scan rate of 25 mV s^{-1}. The obtained results are shown in Fig. S2.† It was observed that no electro-oxidation peak was present in the obtained CV responses, which was due to the absence of hydrazine. In addition, the Ag@ZIF-8/SPE exhibited better catalytic behavior compared to the SPE (Fig. S2†). Thus, we adopted the Ag@ZIF-8-modified SPE as a working electrode for the further hydrazine sensing experiments and studies. The pH of the buffer solution also has significant effects and thus we further obtained CV responses of the Ag@ZIF-8/SPE for 0.5 μM hydrazine in 0.1 M PBS of different pH (3.0, 5.0, 7.0, 9.0, and 11.0). The obtained results are summarized in Fig. S3a.† It can be seen that Ag@ZIF-8/SPE had higher electrocatalytic activity in 0.1 M PBS of pH 7.0 (Fig. S3b†). It is expected that the electron-transfer kinetics would be better at pH 7.0 compared to the other pH levels. Moreover, hydrazine was more stable at neutral pH. Thus, it is also possible that the maximum amount of hydrazine takes part in the electrochemical reactions. Thus, an improved current response was observed at pH 7.0. Therefore, 0.1 M PBS of pH 7.0 was used for all the electrochemical studies.

Since the applied potential scan rate may have significant effects on the electrocatalytic behavior and properties of hydrazine sensors, it would be of great importance to study the effects of the different applied potential scan rates on the electrochemical properties of the Ag@ZIF-8/SPE. The CV curves of the Ag@ZIF-8/SPE were recorded for 0.5 μM hydrazine in 0.1 M PBS (pH 7.0) at different applied scan rates of 25–550 mV s^{-1}. The recorded CVs of the Ag@ZIF-8/SPE at different scan rates are summarized in Fig. 3b. It can be clearly noted that the current response value for the electro-oxidation of hydrazine increased with respect to the applied scan rate. The current response *versus* the square root of the applied scan rate curve is presented in Fig. 3c. A regression coefficient (R^2) value of 0.99 was observed, which suggested that the current response linearly increased with increasing the applied scan rate. In addition, the above results suggested that the electro-oxidation of hydrazine may involve a diffusion-controlled process.

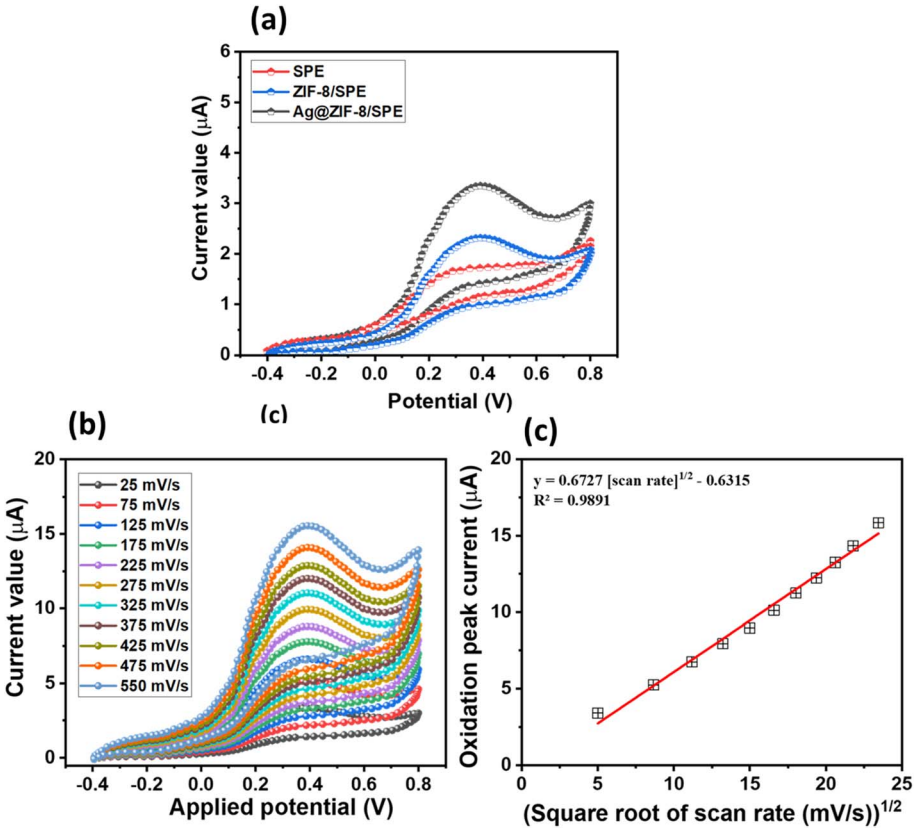

Fig. 3 (a) CV curves of the SPE, ZIF-8/SPE, and Ag@ZIF-8/SPE in the presence of 0.5 μM hydrazine (0.1 M PBS, pH = 7.0) under an applied potential scan rate of 25 mV s^{-1} (b) CV curves of the Ag@ZIF-8/SPE for 0.5 μM hydrazine in 0.1 M PBS (pH = 7.0) at different applied scan rates of 25–550 mV s^{-1}. (c) Calibration plot between the electro-oxidation current peak value and square root of the applied scan rates.

In further studies, we adopted the LSV method for the determination of hydrazine. The LSVs of the SPE, ZIF-8/SPE, and Ag@ZIF-8/SPE were recorded in 0.5 μM hydrazine (prepared in 0.1 M PBS of pH 7.0, scan rate = 25 mV s^{-1}).

It was observed that the electro-oxidation of hydrazine at the surface of SPE exhibited a current response of 3.01 μA, as shown in Fig. 4a. The LSV data of the ZIF-8/SPE also showed some improvements in the electro-oxidation of hydrazine. An improved current response of 5.69 μA was observed for the electro-oxidation of hydrazine at the surface of ZIF-8/SPE whereas a significantly improved current response of 7.23 μA was obtained for Ag@ZIF-8/SPE towards the determination of hydrazine. The concentration of hydrazine may play a vital role and it may affect the electrochemical performance of the Ag@ZIF-8/SPE. In this regard, the LSV responses of the Ag@ZIF-8/SPE were recorded for various concentrations of hydrazine. However, the applied potential scan rate was fixed at 25 mV s^{-1}. The obtained LSVs of the Ag@ZIF-8/SPE for various concentrations of hydrazine are shown in Fig. 4b. The electro-oxidation current response of the Ag@ZIF-8/SPE was increased when the concentration of hydrazine increased. Thus, it is clear that the current response for the electro-oxidation of hydrazine was directly proportional to the concentration of the hydrazine. The current response *versus* concentration of hydrazine plot is presented in Fig. 4c, in which the calibration curve suggested that the current response linearly increased ($R^2 = 0.99$).

Achieving a high selectivity of electrochemical sensors is highly challenging but is a desirable feature for their practical applications. Thus, the selectivity of the Ag@ZIF-8/SPE should be carefully analyzed. In this regard, first, we obtained the LSV curve of the Ag@ZIF-8/SPE in the presence of 0.5 μM hydrazine (scan rate = 25 mV s^{-1}). The obtained results are shown in Fig. 5. Furthermore, a mixture of interfering substances (glucose, hydrogen peroxide, ascorbic acid, *para*-nitrophenol, Cl^-, Na^+, uric acid, urea, citric acid, and ammonia) was spiked in 0.5 μM hydrazine and LSV curves were recorded. The spike amount of interfering species was around five times higher (2.5 μM). The obtained LSV graph of the Ag@ZIF-8/SPE for 0.5 μM hydrazine + 2.5 μM interferences is shown in Fig. 5. It can be seen that there was negligible change in the current variation. This indicated that Ag@ZIF-8/SPE was selective for the detection of hydrazine. Thus, it can be stated that Ag@ZIF-8/SPE possesses good anti-interfering properties and is selective for the sensing of hydrazine.

The sensor reproducibility was checked by modifying 5 SPEs with Ag@ZIF-8 under similar conditions, and the obtained LSV current responses are summarized in Fig. S4a.† The obtained results suggested a decent reproducibility with only a slight change in the current response with a relative stand deviation (r.sd.) of 2.17%. The repeatability of the Ag@ZIF-8/SPE was also checked by employing the LSV method for 50 consecutive cycles. Fig. S4b† shows the good repeatability for 50 cycles with

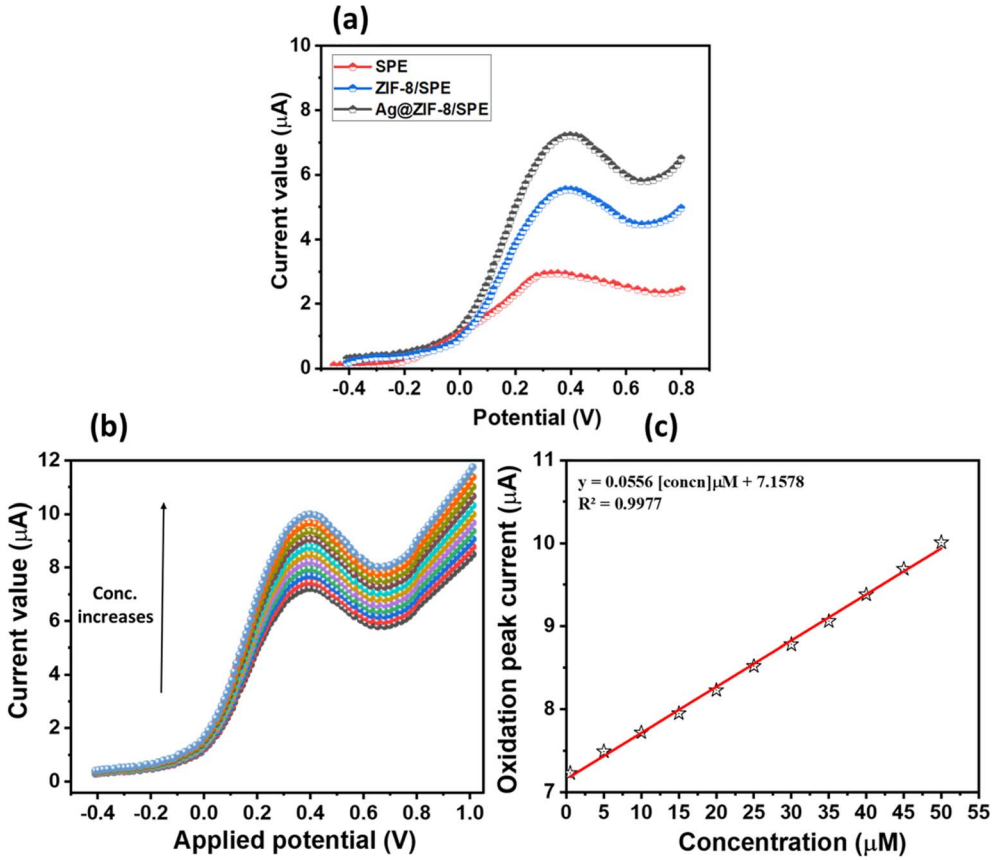

Fig. 4 (a) LSV curves of the SPE, ZIF-8/SPE, and Ag@ZIF-8/SPE in the presence of 0.5 μM hydrazine (0.1 M PBS, pH = 7.0) under an applied potential scan rate of 25 mV s^{-1} (b) LSV curves of the Ag@ZIF-8/SPE for different concentrations (0.5, 5, 10, 15, 20, 25, 30, 35, 40, 45, and 50 μM) of hydrazine in 0.1 M PBS (pH = 7.0) at an applied scan rate of 25 mV s^{-1}. (c) Calibration plot between the electro-oxidation current peak value and the concentration of hydrazine.

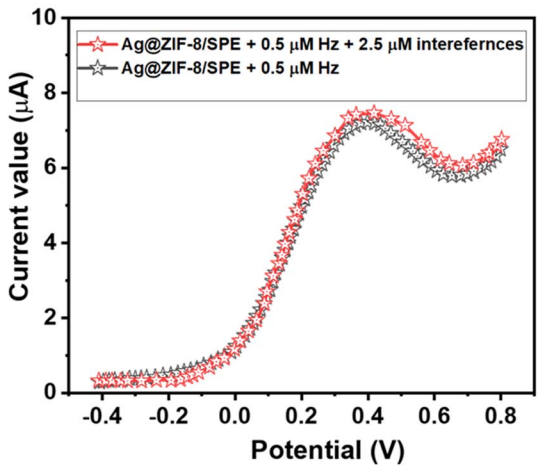

Fig. 5 LSV curves of the Ag@ZIF-8/SPE for 0.5 μM hydrazine and 0.5 μM hydrazine + 2.5 μM interferences (glucose, hydrogen peroxide, ascorbic acid, *para*-nitrophenol, Cl^-, Na^+, uric acid, urea, citric acid, and ammonia) at a scan rate of 25 mV s^{-1}.

an r.s.d. of 3.78%. The storage stability was also studied and the observations revealed that Ag@ZIF-8/SPE had good storage stability of 30 days with an r.s.d. of 3.97%. (Fig. S4c†).

Electrochemical detection *via* the Ag@ZIF-8/SPE surface may involve a two-step electro-oxidation process. The probable mechanism can be described below,[20]

$$N_2H_4 + H_2O \rightarrow N_2H_3 + H_3O^+ + e^- \text{ (slow rate-determine step)} \quad (1)$$

$$N_2H_3 + 3H_2O \rightarrow N_2 + 3H_3O^+ + 3e^- \text{ (fast)} \quad (2)$$

$$N_2H_4 + 4H_2O \rightarrow N_2 + 4H_3O^+ + 4e^- \text{ (overall reaction)} \quad (3)$$

The electrochemical oxidation of hydrazine may generate nitrogen as a product. The probable mechanism has been described as per the previous studies.

The limit of detection, *i.e.*, LoD, of the Ag@ZIF-8/SPE was calculated by employing the formula given below,

$$\text{LoD} = 3 \times \sigma / S_p \quad (4)$$

where σ is the standard error and S_p is the slope of the electrode.

The sensitivity of the Ag@ZIF-8/SPE was determined using the equation below,

$$\text{Sensitivity} = \text{slope of the electrode/working area of the electrode} \quad (5)$$

Table 1 Comparison of the LoD of the Ag@ZIF-8/SPE with published studies[40–54]

Sensor	LoD (μM)	Linear range (μM)	Sensitivity	Technique	Ref.
Ag@ZIF-8/SPE	0.1	0.5 to 50	1.98 μA μM^{-1} cm^{-2}	LSV	This study
Au/Ti	0.042 mM	—	1.117 mA cm^{-2} mM^{-1}	CV	40
Pd/CNF-GCE	2.9	10 to 4000	8.69 mA mM^{-1}	DPV	41
CoOOH nanosheet electrode	20	0 to 1.2 mM	99 μA mM^{-1} cm^{-2}	Amperometry	42
Acetylferrocene-modified carbon paste electrode	2.7×10^{-5} M	3.09×10^{-5} to 1.03×10^{-3} M	—	CV	43
PVP-AgNCs/GCE	1.1	0.005 to 0.46 mM	—	Amperometry	44
ZnO	2.1	3 to 120	15.86 μA mM^{-1}	Amperometry	45
WO_3	144	100 to 1000	0.18,471 μA μM^{-1} cm^2	CV/Amperometry	46
Manganese oxide	2.06	30 μM to 2.83 mM	109.55 μA mM^{-1} cm^{-2}	CV/Amperometry	47
Iron oxide	5	0.1 to 5.5 mM	7.16 μA mM^{-1} cm^{-2}	Amperometry	48
Zirconium dioxide	0.014	2.5×10^{-8} to 5.0×10^{-5} M	—	Chronoamperometry/SWV	49
$NiCoSe_2$ NNA/NF	0.5	—	16 170 μA mM^{-1} cm^{-2}	Amperometry	50
ChAc/ZnO NS/Au	0.4	500–9300 μM	2.66 μA μM^{-1}	LSV	51
CuO NSs/CAB/GCE	0.15	0.5 to 100 μM	—	LSV	52
Ag/L–CPE	1.5	0.01–4 mM	103.13 μA mM^{-1}	Amperometry	53
Pd-Cu-SBA-16/CPE	16	1.79 to 121.86 mM	—	Amperometry	54

Previous years have witnessed various reports on the development of electrode materials for the sensing of hydrazine. In this context, Li *et al.*[40] reported the construction of a hydrazine sensor by employing a gold (Au) nanoparticle-modified titanium (Ti) electrode. Zhang *et al.*[41] fabricated palladium NPs-modified carbon nanofibers for the sensing of hydrazine. In another report, Lee *et al.*[42] used novel strategies for the determination of hydrazine using a CoOOH nanosheet-based electrode for hydrazine sensing. In other works, an acetylferrocene-modified carbon paste electrode,[43] PVP-modified silver nanocubes/GCE,[44] ZnO,[45] tungsten oxide (WO_3),[46] manganese dioxide,[47] iron oxide,[48] zirconium dioxide,[49] $NiCoSe_2$ nanoneedle arrays on nickel foam ($NiCoSe_2$ NNA/NF),[50] choline acetate-modified hexagonal ZnO nanostructure (ChAc/ZnO NS),[51] CuO nanosheets/cellulose,[52] silver-doped zeolite L nanoparticles,[53] and Pd-Cu-SBA-16/CPE[54] were explored as hydrazine sensors. The performance of the reported sensors and that of the sensor in the present study (Ag@ZIF-8/SPE) are summarized in Table 1.

Real-sample investigations were also carried out using the LSV technique. The standard spike addition method was adopted for the real-sample investigations. The performance of the Ag@ZIF-8/SPE was checked in tap water. Tap water was used as the control and different amounts (0, 0.5, and 1.0 μM) of hydrazine were spiked and their performance was determined using LSV. The obtained results are summarized in Table 2. The observations suggested the good performance of the Ag@ZIF-8/SPE for real-sample investigations.

Table 2 Recovery of hydrazine in water samples using the standard spike addition method

Tap water	Added (μM)	Found (μM)	Recovery (%)
Hydrazine	0	0	0
	0.5	0.48	96
	1.0	0.97	97

4. Conclusions

In conclusion, we synthesized Ag@ZIF-8 *via* a simple synthetic approach. The synthesized Ag@ZIF-8 was characterized by XRD and SEM methods, while the presence of Ag was checked by the EDX approach. Furthermore, the SPE surface was coated with the synthesized Ag@ZIF-8 catalyst. The modified SPE (Ag@ZIF-8/SPE) was introduced and assessed as a hydrazine sensor. The Ag@ZIF-8/SPE exhibited a good detection limit and selectivity with reasonable sensitivity. The Ag@ZIF-8/SPE also demonstrated good stability and repeatability. This work proposes the synthesis of Ag@ZIF-8 as a catalyst and the fabrication of a simple and eco-friendly hydrazine sensor.

Data availability

All the data figures are present in the manuscript.

Conflicts of interest

There are no conflicts to declare.

Acknowledgements

Authors gratefully acknowledged Researchers Supporting Project number (RSP2025R400), King Saud University, Riyadh, Saudi Arabia.

References

1 M. Sun, L. Bai and D. Q. Liu, A generic approach for the determination of trace hydrazine in drug substances using *in situ* derivatization-headspace GC-MS, *J. Pharm. Biomed. Anal.*, 2009, **49**(2), 529–533.
2 L. J. Tang, L. Zhou, A. J. Liu, X. M. Yan, K. L. Zhong, X. Y. Liu, X. Gao and J. R. Li, A new cascade reaction-based

colorimetric and fluorescence "turn on" dual-function probe for cyanide and hydrazine detection, *Dyes Pigm.*, 2021, **186**, 109034.

3 D. M. Nguyen, L. G. Bach and Q. B. Bui, Novel urchin-like FeCo oxide nanostructures supported carbon spheres as a highly sensitive sensor for hydrazine sensing application, *J. Pharm. Biomed. Anal.*, 2019, **172**, 243–252.

4 K. Ahmad, M. Q. Khan, A. Alsulmi and H. Kim, Synthesis of tin oxide (SnO_2) for the fabrication of voltammetric hydrazine sensor, *Mater. Chem. Phys.*, 2023, **302**, 127702.

5 C. Batchelor-McAuley, C. E. Banks, A. O. Simm, T. G. J. Jones and R. G. Compton, The electroanalytical detection of hydrazine : a comparison of the use of palladium nanoparticles supported on boron-doped diamond and palladium plated BDD microdisc array, *Analyst*, 2006, **131**, 106–110.

6 X. Yan, F. Meng, S. Cui, J. Liu, J. Gu and Z. Zou, Effective and rapid electrochemical detection of hydrazine by nanoporous gold, *J. Electroanal. Chem.*, 2011, **661**, 44–48.

7 S. Garrod, M. E. Bollard, A. W. Nicholls, S. C. Connor, J. Connelly, J. K. Nicholson and E. Holmes, Integrated metabonomic analysis of the multiorgan effects of hydrazine toxicity in the rat, *Chem. Res. Toxicol.*, 2005, **18**, 115–122.

8 S. Tafazoli, M. Mashregi and P. J. O'Brien, Role of hydrazine in isoniazid-induced hepatotoxicity in a hepatocyte inflammation model, *Toxicol. Appl. Pharmacol.*, 2008, **229**, 94–101.

9 H. M. A. Amin, M. F. El-Kady, N. F. Atta and A. Galal, Gold nanoparticles decorated graphene as a high performance sensor for determination of trace hydrazine levels in water, *Electroanalysis*, 2018, **30**, 1757–1766.

10 U. Ragnarsson, Synthetic methodology for alkyl substituted hydrazines, *Chem. Soc. Rev.*, 2001, **30**, 205–213.

11 S. Tajik, H. Beitollahi, S. Zia Mohammadi, M. Azimzadeh, K. Zhang, Q. V. Le, Y. Yamauchi, H. Won Jang and M. Shokouhimehr, Recent developments in electrochemical sensors for detecting hydrazine with different modified electrodes, *RSC Adv.*, 2020, **10**, 30481–30498.

12 S. H. Kazemi, B. Hosseinzadeh and S. Zakavi, Electrochemical fabrication of conducting polymer of Ni-porphyrin as nano-structured electrocatalyst for hydrazine oxidation, *Sens. Actuators, B*, 2015, **210**, 343–348.

13 S. Rani, S. Kapoor, B. Sharma, S. Kumar, R. Malhotra and N. Dilbaghi, Fabrication of Zn-MOF@rGO based sensitive nanosensor for the real time monitoring of hydrazine, *J. Alloys Compd.*, 2020, **816**, 152509.

14 L. Song, D. Gao, S. Li, Y. Wang, H. Liu and Y. Jiang, Simultaneous quantitation of hydrazine and acetylhydrazine in human plasma by high performance liquid chromatography-tandem mass spectrometry after derivatization with ptolualdehyde, *J. Chromatogr. B*, 2017, **1063**, 189–195.

15 K. McAdam, H. Kimpton, S. Essen, P. Davis, C. Vas, C. Wright, A. Porter and B. Rodu, Analysis of hydrazine in smokeless tobacco products by gas chromatography–mass spectrometry, *Chem. Cent. J.*, 2015, **9**, 13.

16 B. Li, Z. Zhang and M. Wu, Flow-injection chemiluminescence determination of captopril using on-line electrogenerated silver(II) as the oxidant, *Microchem. J.*, 2001, **70**, 85–91.

17 M. George, K. S. Nagaraja and N. Balasubramanian, Spectrophotometric determination of hydrazine, *Talanta*, 2008, **75**, 27–31.

18 J. Fan, J. Kong, S. Feng, J. Wang and P. Peng, Kinetic fluorimetric determination of trace hydrazine in environmental waters, *J. Environ. Anal. Chem.*, 2006, **86**, 995–1005.

19 H. Zare and A. Habibirad, Electrochemistry and electrocatalytic activity of catechinfilm on a glassy carbon electrode toward the oxidation of hydrazine, *J. SolidState Electrochem.*, 2006, **10**, 348–359.

20 A. Mohammad, M. E. Khan, I. M. Alarifi, M. H. Cho and T. Yoon, A sensitive electrochemical detection of hydrazine based on SnO_2/CeO_2 nanostructured oxide, *Microchem. J.*, 2021, **171**, 106784.

21 J. Li and X. Lin, Electrocatalytic oxidation of hydrazine and hydroxylamine at goldnanoparticle—polypyrrole nanowire modified glassy carbon electrode, *Sens. Actuators, B*, 2007, **126**, 527–535.

22 S. Ivanov, U. Lange, V. Tsakova and V. M. Mirsky, Electrocatalytically activenanocomposite from palladium nanoparticles and polyaniline: oxidation ofhydrazine, *Sens. Actuators, B*, 2010, **150**, 271–278.

23 A. Salimi and K. Abdi, Enhancement of the analytical properties and catalyticactivity of a nickel hexacyanoferrate modified carbon ceramic electrode pre-pared by two-step sol–gel technique: application to amperometric detectionof hydrazine and hydroxyl amine, *Talanta*, 2004, **63**, 475–483.

24 H. Qiu, L. Xue, G. Ji, G. Zhou, X. Huang, Y. Qu, *et al.*, Enzyme-modifiednanoporous gold-based electrochemical biosensors, *Biosens. Bioelectron.*, 2009, **24**, 3014–3018.

25 A. Guzmán-Vargas, M. A. Oliver-Tolentino, E. Lima and J. Flores-Moreno, Efficient electrocatalytic reduction of nitrite species on zeolite modified electrode withCu-ZSM-5, *Electrochim. Acta*, 2013, **108**, 583–590.

26 F. Wu, L.-G. Qiu, F. Ke and X. Jiang, Copper nanoparticles embedded inmetal–organic framework MIL-101(Cr) as a high performance catalyst for reduction of aromatic nitro compounds, *Inorg. Chem. Commun.*, 2013, **32**, 5–8.

27 H.-C. Zhou, J. R. Long and O. M. Yaghi, Introduction to metal–organic frameworks, *Chem. Rev.*, 2012, **112**, 673–674.

28 O. K. Farha and J. T. Hupp, Rational design, synthesis, purification, and activation ofmetal−organic framework materials, *Acc. Chem. Res.*, 2010, **43**, 1166–1175.

29 M. Sabo, A. Henschel, H. Frode, E. Klemm and S. Kaskel, Solution infiltration of pal-ladium into MOF-5: synthesis, physisorption and catalytic properties, *J. Mater.Chem.*, 2007, **17**, 3827–3832.

30 C. Zhang, M. Wang, L. Liu, X. Yang and X. Xu, Electrochemical investigation of a newCu-MOF and its

electrocatalytic activity towards H_2O_2 oxidation in alkalinesolution, *Electrochem. Commun.*, 2013, **33**, 131–134.

31 A. M. Balu, C. S. K. Lin, H. Liu, Y. Li, C. Vargas and R. Luque, Iron oxide functionalized MIL-101 materials in aqueous phase selective oxidations, *Appl. Catal., A*, 2013, **455**, 261–266.

32 R. Banerjee, A. Phan, B. Wang, C. Knobler, H. Furukawa, M. O'Keeffe, *et al.*, High-throughput synthesis of zeolitic imidazolate frameworks and application to CO2 capture, *Science*, 2008, **319**, 939–943.

33 C. Chen, J. Kim, D.-A. Yang and W.-S. Ahn, Carbon dioxide adsorption over zeolite-like metal organic frameworks (ZMOFs) having a sod topology: structure andion-exchange effect, *Chem. Eng. J.*, 2011, **168**, 1134–1139.

34 G. Lu and J. T. Hupp, Metal–organic frameworks as sensors: a ZIF-8 based Fabry–Pérot device as a selective sensor for chemical vapors and gases, *J. Am. Chem. Soc.*, 2010, **132**, 7832–7833.

35 R. Huang, K. Zhang, H. Sun, D. Zhang, J. Zhu, S. Zhou, W. Li, Y. Li, C. Wang, X. Jia, T. Wågberg and G. Hu, Star-shaped porous nitrogen-doped metal-organic framework carbon as an electrochemical platform for sensitive determination of Cd(II) in environmental and tobacco samples, *Anal. Chim. Acta*, 2022, **1228**, 340309.

36 B. Fatima, D. Hussain, A. Saeed, *et al.*, Tellurium doped zinc imidazole framework (Te@ZIF-8) for quantitative determination of hydrogen peroxide from serum of pancreatic cancer patients, *Sci. Rep.*, 2020, **10**, 21077.

37 M. Usman and M. H. Suliman, Silver-Doped Zeolitic Imidazolate Framework (Ag@ZIF-8): An Efficient Electrocatalyst for CO2 Conversion to Syngas, *Catalysts*, 2023, **13**, 867.

38 J. Abdi, Synthesis of Ag-doped ZIF-8 photocatalyst with excellent performance for dye degradation and antibacterial activity, *Colloids Surf., A*, 2020, **604**, 125330.

39 J. Li, H. Chang, Y. Li, Q. Li, K. Shen, H. Yi and J. Zhang, Synthesis and adsorption performance of La@ZIF-8 composite metal–organic frameworks, *RSC Adv.*, 2020, **10**, 3380–3390.

40 Q. Yi and W. Yu, Nanoporous gold particles modified titanium electrode for hydrazine oxidation, *J. Electroanal. Chem.*, 2009, **633**, 159–164.

41 H. Zhang, J. Huang, H. Hou and T. You, Electrochemical detection of hydrazine based on electrospun palladium nanoparticle/carbon nanofibers, *Electroanalysis*, 2009, **21**, 1869–1874.

42 K. K. Lee, P. Y. Loh, C. H. Sow and W. S. Chin, COOOH nanosheet electrodes: simple fabrication for sensitive electrochemical sensing of hydrogen peroxide and hydrazine, *Biosens. Bioelectron.*, 2013, **39**, 255–260.

43 R. Ojani, J.-B. Raoof and B. Norouzi, Acetylferrocene modified carbon paste electrode: a sensor for electrocatalytic determination of hydrazine, *Electroanalysis*, 2008, **20**, 1378–1382.

44 Y. Wang, X. Yang, J. Bai, X. Jiang and G. Fan, High sensitivity hydrogen peroxide and hydrazine sensor based on silver nanocubes with rich {1 0 0} facets as an enhanced electrochemical sensing platform, *Biosens. Bioelectron.*, 2013, **43**, 180–185.

45 Y. Ni, J. Zhu, L. Zhang and J. Hong, Hierarchical ZnO micro/nanoarchitectures: hydrothermal preparation, characterization and application in the detection of hydrazine, *CrystEngComm*, 2010, **12**, 2213–2218.

46 S. Shukla, S. Chaudhary, A. Umar, G. R. Chaudhary and S. K. Mehta, Tungsten oxide (WO_3) nanoparticles as scaffold for the fabrication of hydrazine chemical sensor, *Sens. Actuators, B*, 2014, **196**, 231–237.

47 J. Wu, T. Zhou, Q. Wang and A. Umar, Morphology and chemical composition dependent synthesis and electrochemical properties of MnO_2-based nanostructures for efficient hydrazine detection, *Sens. Actuators, B*, 2016, **224**, 878–884.

48 S. Majumder, B. Saha, S. Dey, R. Mondal, S. Kumar and S. Banerjee, A highly sensitive non-enzymatic hydrogen peroxide and hydrazine electrochemical sensor based on 3D micro-snowflake architectures of α-Fe_2O_3, *RSC Adv.*, 2016, **6**, 59907–59918.

49 S. Z. Mohammadi, H. Beitollahi and B. E. Asadi, Electrochemical determination of hydrazine using a ZrO_2 nanoparticles-modified carbon paste electrode, *Environ. Monit. Assess.*, 2015, **187**, 122.

50 Y. Xing, X. Tang, C. Ling, Yu Zhang, Z. He, G. Ran, H. Yu, Ke Huang, Z. Zou and X. Xiong, Three-dimensional Setaria viridis-like $NiCoSe_2$ nanoneedles array: As an efficient electrochemical hydrazine sensor, *Colloids Surf., A*, 2022, **650**, 129549.

51 A. Kaur, U. Chakraborty, M. Chauhan, R. Sharma, G. Kaur and G. R. Chaudhary, Choline acetate modified ZnO nanostructure as efficient electrochemical sensor for hydrazine detection, *Electrochim. Acta*, 2022, **419**, 140384.

52 N. Alahmadi, H. S. Alhasan, H. Gomaa, A. A. Abdelwahab and M. Y. Emran, Electrochemical sensor design based on CuO nanosheets/Cellulose derivative nanocomposite for hydrazine monitoring in environmental samples, *Microchem. J.*, 2022, **183**, 107909.

53 N. S. Gilani, S. N. Azizi and S. Ghasemi, Sensitive amperometric determination of hydrazine using a carbon paste electrode modified with silver-doped zeolite L nanoparticles, *Bull. Mater. Sci.*, 2017, **40**, 177–185.

54 S. Kavian, S. N. Azizi and S. Ghasemi, Novel bimetallic nanoporous Pd-Cu-SBA-16/CPE as a highly sensitive sensor for determination of formaldehyde, *J. Electroanal. Chem.*, 2017, **799**, 308–314.